Original Scientific Paper

Lab Report

Qiyu Liu[1]

[1] *UCLA*

E–mail: *liuleo184@g.ucla.edu*

Abstract

This report details the implementation of quantum computing algorithms on a nuclear magnetic resonance (NMR) system using chloroform molecules as qubits. The theoretical background of NMR quantum computing is covered, including state preparation, quantum gate decomposition into pulse sequences, and the specific properties of the chloroform sample. Experiments are performed to demonstrate the realization of the CNOT gate, the Deutsch-Jozsa algorithm for distinguishing constant and balanced binary functions, and Grover's search algorithm. The pulse sequences designed for each algorithm are translated onto the NMR system, and the experimental results are analyzed by comparing the final spectra to simulations. Grover's periodic behaviour is also implemented and proven. Challenges such as noise and accumulated error from increased circuit complexity are discussed. The GitHub repository containing the simulation and pulse sequence code is provided for reference.

Key words. Nuclear Magnetic Resonance - Deutsch-jozsa - Grover

1. Introduction

The advent of quantum computing marks a revolutionary leap forward from classical computing paradigms, promising unprecedented computational power and efficiency. This emerging field seeks to harness the principles of quantum mechanics to perform complex computations at speeds unattainable by today's most advanced supercomputers. Among the various physical systems being explored for quantum computation, liquid-state Nuclear Magnetic Resonance (NMR) has carved out a niche due to its unique advantages. Liquid NMR, a technique well-established in the realms of chemistry and medicine for molecule characterization, has been repurposed with innovative flair to pioneer early quantum computing efforts. The high degree of control over spin states, coupled with the ability to manipulate them using radiofrequency pulses, makes liquid NMR an attractive testbed for quantum algorithms.

The utilization of liquid NMR for quantum computing aligns with the field's overarching goal: to achieve quantum supremacy, where quantum devices perform tasks that classical computers fundamentally cannot. In this context, we focus on implementing two seminal quantum algorithms—the Deutsch-Jozsa and Grover algorithms—using an NMR apparatus. These algorithms not only highlight the potential of quantum computing to solve specific problems more efficiently than classical approaches but also serve as benchmarks for the capabilities of quantum systems.

Our exploration into NMR-based quantum computing is motivated by both the technical challenges and the potential it holds for future advancements. The ability to prepare pseudo-pure states and execute quantum gates in a controlled NMR environment paves the way for more complex quantum computations. However, the inherent limitations of the NMR approach, including scalability and noise issues, present hurdles that must be overcome to realize the full promise of quantum computing.

As we stand on the cusp of a new computational era, the journey of liquid NMR in the quantum domain exemplifies the innovative repurposing of existing technologies to explore the quantum frontier. This study not only contributes to our understanding of quantum algorithm implementation in NMR systems but also offers insights into the challenges that lie ahead. By addressing these challenges, we move closer to a future where quantum computing

can solve some of the world's most pressing problems, from drug discovery to climate modeling, with unprecedented speed and precision.

2. NMR with Chloroform

A qubit, short for quantum bit, is the basic unit of quantum information and characterized by a two-level quantum system. They are usually labeled as $|0\rangle$ and $|1\rangle$, in the σ_z computational basis by convention. Unlike classical bits, they are not restricted to being in just one of the computational basis states. It is mathematically represented as $|\psi\rangle = \alpha|0\rangle + \beta|1\rangle$. The coefficients α and β are complex numbers that describe the probability amplitudes of the qubit's state, with the condition that $|\alpha|^2+|\beta|^2 = 1$. This superposition, along with entanglement, enables quantum computers to process information in ways fundamentally different from classical computers.

Since a qubit is a two-level system, it is natural to implement them with a spin-$\frac{1}{2}$ nucleus. Similarly, for a two-qubit system, we resort to molecules with two spin-$\frac{1}{2}$ nuclei with distinct energy spectra so that we can individually control them [2]. In addition, there needs to be interaction between the two nuclei so that two-qubit logic gates can be implemented.

2.1. Control

To utilize NMR systems for quantum computing, we must develop methods to precisely control the state of the qubits. Conventionally, an applied magnetic field along the z-direction establishes the computational z-basis reference. The Hamiltonian under this field is given by

$$\hat{H} = \frac{\omega_0}{2}\hat{\sigma}_z,$$

where σ_z is the Pauli-z operator, and ω_0 is the energy splitting of the nucleus, or the Larmor frequency.

To manipulate the qubit, we introduce a time-dependent sinusoidal drive

$$\hat{H} = \frac{\omega_0}{2}\hat{\sigma}_z + \Omega\cos(\omega t + \phi)\hat{\sigma}_x,$$

in the x-direction. To simplify the visualization of this drive's behavior by rendering the time-dependent part of the Hamiltonian stationary, we transform our Hamiltonian into the rotating frame:

$$\hat{H} = \frac{\delta}{2}\hat{\sigma}_z + \frac{\Omega}{2}\hat{\sigma}_x,$$

where δ denotes the detuning between the drive and Larmor frequency. If the drive is in exact resonance with the Larmor frequency, then the Hamiltonian simplifies to only include the $\hat{\sigma}_x$ term, laying the groundwork for our control mechanisms and quantum gates. A similar concept applies when driving in the y-direction, utilizing the Pauli operator $\hat{\sigma}_y$.

By adjusting the phase, duration, and timing of the RF pulse, we can manipulate the states. These parameters facilitate the rotation of the qubit state on the Bloch sphere, enabling operations such as bit flips (X gates) and phase shifts (Z gates). The capability to execute these operations with high precision is essential for implementing quantum algorithms.

2.2. Chloroform's Properties

Our Nuclear Magnetic Resonance system uses Chloroform molecules as a two-qubit quantum computing system. The Hamiltonian is given below as

$$\hat{H} = \Omega_I\hat{I}_z + \Omega_S\hat{S}_z + 2\pi J_{IS}\hat{I}_z\hat{S}_z,$$

The $\hat{I}_z$ represents the hydrogen term, $\hat{S}_z$ represents the carbon term, and $\hat{I}_z\hat{S}_z$ represents the J-coupling term between hydrogen and carbon [3]. This J-coupling between hydrogen proton ^1H and carbon ^{13}C nuclei arises from indirect electron-mediated interactions, causing NMR signal splitting. This scalar coupling reflects the nuclei's spatial arrangement and electron distribution, crucial for analyzing molecular structure.

As we know, the ^1H and ^{13}C inside Chloroform are both spin-$\frac{1}{2}$ particles and have distinct energy spectra so that we can individually control them. Their Hamiltonian also indicates that they have interaction between them so that we can utilize this fact to implement two-qubits logic gates.

To precisely control the qubit, we need to know a few properties about the carbon and hydrogen in our chloroform sample. We want to know the $\frac{\pi}{2}$ control pulse pulse length for each channel. Moreover, we need to know the center frequency of each channel so that our RF pulsing signal is at the right frequency. The J coupling coefficient is also important for implementing two-qubit control gates. Last but not least, the T_1 relaxation time is essential to know if we want to repeat the experiment, since we want the system to fully relax back to the original state.

- **Pulse Length:** The pulse length needs to be calibrated to ensure we have an optimal control sequence for rotating our magnetization on the Bloch sphere. To find the optimal $\frac{\pi}{2}$ pulse length, we run the Free Induction Decay (FID) experiment with an iteratively small increment list of pulse lengths. The optimal $\frac{\pi}{2}$ pulse length should be the one that corresponds to the maximal signal strength, which we can obtain from integrating the frequency spectrum peaks. We found that the optimal pulse length is 12.6 μs.

- **J-coupling Strength:** The J-coupling term contributes to the interaction between ^1H and ^{13}C. This value is critical for our implementation of two-qubit gates. To measure the J-coupling coefficient, we measure the difference

between two peaks after running the FID experiment for either channel. For our system, the J-coupling coefficient is about 215 Hz.

- T_1 **Relaxation Time:** When we apply an RF pulse, we change the magnetization of the NMR system. However, when the RF pulse disappears, the magnetization will return to the equilibrium point toward the z-direction (B_0 field). Knowing this relaxation time is essential for repeating the experiments. We can use the inversion recovery algorithm and fit the signal strength with the relationship

$$S(t) = S_0(1 - 2e^{-\frac{t}{T_1}})$$

which allow us to extract the T_1 time. To allow the system to fully relax to the original thermal state, we allow for $5T_1$ repeat ion time in between scans of experiments.

2.3. Quantum gates as pulse sequence

In the realm of quantum computing, computer scientists often abstract away the complexities of the physical system to focus on computational models and algorithms. By drawing analogies to classical computers, they utilize quantum gates, mathematically represented by unitary matrices, to model operations within quantum computing circuits. These quantum gates allow for the manipulation of qubits, the fundamental units of quantum information, enabling the construction of circuits with capabilities far beyond those of classical computers.

One of the key strengths of quantum computing lies in its ability to perform tasks that are infeasible for classical computers, such as prime factorization and unstructured search, with significantly greater efficiency. This efficiency is achieved through the coherent superposition and entanglement of qubits, properties unique to quantum mechanics.

For systems based on Nuclear Magnetic Resonance (NMR), the realization of quantum gates can be achieved by carefully pulsing the system and observing the time evolution operator under these pulses. The NMR approach to quantum computing leverages the spin states of atomic nuclei within molecules as qubits, with the manipulation of these states through radio frequency (RF) pulses corresponding to the application of quantum gates.

The procedure for implementing quantum gates in NMR is as follows. For a given time-independent Hamiltonian $\hat{H}$, the time evolution operator is given by

$$\hat{U}(t) = e^{-\frac{i\hat{H}t}{\hbar}}$$

which means that the final state of the qubit will be given by $\hat{U}(t)\,|\psi_0\rangle$. Therefore, we can design and tailor our Hamiltonian with control pulses to realize $\hat{U}(t)$ that matches the quantum gates requested by computer scientists.

The essential quantum gates used in constructing NMR-based quantum circuits include:

- **X Gate (Pauli-X, Quantum NOT Gate):** Represented by the matrix $\begin{pmatrix} 0 & 1 \\ 1 & 0 \end{pmatrix}$, the X gate flips the state of a qubit, analogous to the classical NOT gate.

$$\hat{U} = e^{-i\hat{I}_x\pi} = X$$

The X-gate can be achieved by applying R_x pulses for π duration up to a global phase difference

- **H Gate (Hadamard Gate):** The Hadamard gate, represented by the matrix $\frac{1}{\sqrt{2}}\begin{pmatrix} 1 & 1 \\ 1 & -1 \end{pmatrix}$, facilitates the creation of superpositions, enabling a qubit to simultaneously exist in a combination of basis states. The realization of the H gate can be achieved through the composition of three time evolution operators, expressed as:

$$\hat{U} = e^{i\hat{I}_y\pi/4}e^{-i\hat{I}_x\pi}e^{-i\hat{I}_y\pi/4} = H$$

This sequence demonstrates that the H gate can be effectively implemented by orchestrating radio frequency (RF) pulses along the x and y axes, specifically through the sequence:

$$(r_y(\pi/4)) - (r_x(\pi)) - (r_y(-\pi/4))$$

- **CZ Gate (Controlled-Z):** The Controlled-Z (CZ) gate introduces a phase shift to the target qubit exclusively when the control qubit is in the state $|1\rangle$. It is mathematically depicted by the matrix

$$CZ = \begin{pmatrix} 1 & 0 & 0 & 0 \\ 0 & 1 & 0 & 0 \\ 0 & 0 & 1 & 0 \\ 0 & 0 & 0 & -1 \end{pmatrix}$$

for two qubits. Owing to the constraints of NMR systems that preclude direct pulsing in the z-direction, a composite pulse strategy is adopted to replicate the desired outcome. The sequence

$$[I_x(-\pi/2) - I_y(\pi/2) - I_x(\pi/2)]$$

is implemented to simulate the z-directional influence effectively. The exhaustive pulse sequence to realize the CZ gate, while accommodating the NMR system's limitations, is detailed as follows:

$$\begin{aligned}[I_x(-\pi/2) - I_y(\pi/2) - I_x(\pi/2)] - \\ [S_x(-\pi/2) - S_y(\pi/2) - S_x(\pi/2)] - \\ [IzSz(\pi)]\end{aligned}$$

The $[IzSz(\pi)]$ pulse represents the time evolution of the J-coupling term, described by

$$\hat{U} = e^{-i\hat{I}_z\hat{S}_z\pi},$$

in the rotating frame, and can be implemented by allowing the system to evolve naturally. Given the J-coupling coefficient of 215 Hz, the duration required for this evolution to implement the pulse is $\frac{1}{2J} = 2.32\ ms$. The time evolution operator resulting from this entire pulse sequence successfully emulates the CZ gate up to a global phase factor, as verified in QuTiP. A link to the GitHub repository containing this verification is provided in the Appendix.

- **CNOT Gate (Controlled-NOT):** The Controlled-NOT (CX) gate alters the state of the target qubit only if the control qubit is in the state $|1\rangle$. This operation is mathematically represented by the matrix

$$CX = \begin{pmatrix} 1 & 0 & 0 & 0 \\ 0 & 1 & 0 & 0 \\ 0 & 0 & 0 & 1 \\ 0 & 0 & 1 & 0 \end{pmatrix}$$

for two qubits. The implementation of the CX gate can be achieved by surrounding the CZ gate with two Hadamard gates applied to the target qubit. Mathematically, this relationship is expressed as

$$(I \otimes H) \cdot CZ \cdot (I \otimes H) = CX,$$

where I is the identity matrix representing the operation on the control qubit, and H is the Hadamard gate applied to the target qubit. Given the implementations of both H and CZ gates as previously described, we can concatenate their respective pulse sequences to construct the CNOT gate within an NMR system.

2.4. Pseudo Pure state preparation

Another important aspect of realizing quantum computing on an NMR machine is the ability to prepare the $|00\rangle$ state within the system. Initially, our system is in the thermal state governed by the equation

$$\rho_{\text{th}} = \frac{1}{Z}e^{-\beta\hat{H}},$$

where $\beta = \frac{1}{k_B T}$ and $\hat{H}$ is our Hamiltonian of the NMR system. Since all NMR observables are traceless, we can extract the identity component from the density matrix, allowing us to focus on the deviation density matrix [4]. To construct the pure state $|00\rangle$, we introduce three permutation matrices P_0, P_1, and P_2. Here, P_0 serves as the identity matrix, while P_1 and P_2 are defined as

$$P_1 = \begin{pmatrix} 1 & 0 & 0 & 0 \\ 0 & 0 & 1 & 0 \\ 0 & 0 & 0 & 1 \\ 0 & 1 & 0 & 0 \end{pmatrix}, \quad \text{and} \quad P_2 = \begin{pmatrix} 1 & 0 & 0 & 0 \\ 0 & 0 & 0 & 1 \\ 0 & 1 & 0 & 0 \\ 0 & 0 & 1 & 0 \end{pmatrix}.$$

By applying permutation averaging to eliminate undesirable input states, we achieve

$$\bar{\rho} = \frac{1}{3}\sum_i P_i \rho_{\text{th}} P_i^\dagger = \alpha\hat{I} + \beta\,|00\rangle\langle 00|\,,$$

where α and β represent the coefficients of the identity and pseudo-pure state components of the density matrix, respectively. Given that NMR signals are inherently traceless, this process effectively accomplishes the preparation of a pure state within an NMR machine.

3. Deutsch-jozsa and Grover Algorithms

The Deutsch-Jozsa and Grover algorithms are two cornerstone quantum algorithms demonstrating quantum computing's superiority over classical approaches in specific scenarios. The Deutsch-Jozsa algorithm efficiently determines if a binary function is constant (same output for every input) or balanced (equal number of zeros and ones as outputs), showcasing quantum parallelism by solving the problem with just one query. This contrasts sharply with classical methods, which require multiple queries.

Grover's algorithm, in contrast, tackles the challenge of searching through an unsorted database. It achieves a significant speedup by finding the desired item with $O(\sqrt{N})$ queries, compared to the classical approach's $O(N)$ queries, where N is the database size. This quadratic improvement illustrates quantum computing's potential to revolutionize fields reliant on search and optimization tasks, emphasizing its ability to handle problems previously deemed computationally infeasible.

3.1. Deutsch-jozsa theory

For our two-qubit system, there are four possible oracle functions. In Table 1, the four possible classical functions for our two-qubit system are listed. For the Deutsch-Jozsa algorithm, the overall structure is shown in Figure 1. To implement the different cases of classical functions listed in Table 1, we need different oracles.

The f_0 oracle is empty; the f_1 oracle is a single X gate on q_1; the f_2 oracle has a CNOT gate with control on q_0 and target on q_1; the f_3 oracle has an X gate before and after the CNOT gate on q_0. Simulation shows that by utilizing the quantum circuit and measuring the output states, we can identify the type of the function f.

Simulating the four circuits in Qiskit, the respective density matrix for the two constant functions are

$$\rho_{\text{const}} = \begin{pmatrix} 1 & 0 & 0 & 0 \\ 0 & 0 & 0 & 0 \\ 0 & 0 & 0 & 0 \\ 0 & 0 & 0 & 0 \end{pmatrix},$$

and the density matrix for the two balanced functions are

$$\rho_{\text{balance}} = \begin{pmatrix} 0 & 0 & 0 & 0 \\ 0 & 1 & 0 & 0 \\ 0 & 0 & 0 & 0 \\ 0 & 0 & 0 & 0 \end{pmatrix}.$$

And we see that the constant cases will measure $|0\rangle$ for q_0 and balances cases will measure $|1\rangle$ for q_0. To determine if our NMR system is capable of producing equivalent results, we must translate the quantum circuits into pulse sequences, adhering to the guidelines delineated in the preceding section. By examining the final spectrum of our NMR outputs, we shall be able to discern the final states following the execution of the Deutsch-Jozsa algorithm on our NMR apparatus. The pulse sequences corresponding to the algorithms will be uploaded to github.

Oracles	Function Type	$f(0)$	$f(1)$
f_0	Constant Zero	0	0
f_1	Constant One	1	1
f_2	Balanced One	0	1
f_3	Balanced Two	1	0

Table 1: Classical Constant and Balanced Functions from f_0 to f_3.

3.2. Grover Theory

In our implementation of Grover's algorithm, we have selected a classical function defined as:

$$f(x) = \begin{cases} 1 & \text{if } x = 11, \\ 0 & \text{otherwise.} \end{cases}$$

This function is crucial for demonstrating the algorithm's ability to pinpoint the marked state $|11\rangle$ among a set of possible states. The execution of this particular instantiation of Grover's algorithm is depicted in Figure 2. Simulations performed in Qiskit verify that this circuit indeed results in $-|11\rangle$ as the final state vector, confirming the successful identification of the target state.

The Grover operator, when expressed in state vector format, is given by $\hat{G} = \hat{H}^{\otimes 2}\hat{P}\hat{H}^{\otimes 2}\hat{O}$. Application of this operator to the state indicates that the probability of measuring the solution space $|S\rangle$ is governed by $\sin((2k+1)\theta)$, where $\theta = \arcsin\frac{1}{2} = \frac{\pi}{6}$. Consequently, the probability of measuring the solution is captured by the expression

$$\sin((2k+1)\frac{\pi}{6})$$

revealing that the probability amplitude achieves a maximum of 1 with a period of 3. Therefore, optimal measurement of the solution state is anticipated upon repeating the algorithm 4, 7, and 10 times.

To verify whether our NMR system can replicate these findings, it is imperative to translate the quantum circuits into pulse sequences, adhering to the methodologies described in the preceding sections. An examination of the final spectrum obtained from our NMR outputs will facilitate the validation of the resultant states following the Grover algorithm's execution on our NMR setup. The detailed pulse sequences for the algorithms will be made accessible on GitHub.

4. Experiment and Analysis

A few parameters for all the following experiments are outlined here. Center frequencies are 6.5 and 75 ppm for hydrogen and carbon. Pulse lengths are 12.6 and 78 for hydrogen and carbon. The free evolution is 2.32 ms. We are taking 32,000 points for hydrogen with a dwell time of 200 μs.

4.1. Approximate CNOT and CNOT

Following the theoretical discussions on pulse sequences, we have implemented both the approximate and exact CNOT gates on our NMR machine, initiating from the thermal state. As evidenced by Figures 3 and Figures 4, it is observed that both the approximate and exact CNOT gates produce analogous effects on the thermal state.

The frequency spectrum plots closely mirror the anticipated shapes and patterns derived from our simulations. To acquire a more accurate understanding, we also integrated the frequency peaks, considering that peak heights alone may sometimes yield a misleading representation. For both the CNOT and its approximate counterpart, the integrals of the frequency areas are well-aligned with the ratios observed in the simulation results.

The only notable distinction between the exact CNOT and the Approximate CNOT lies in the broadening of the linewidth observed in the spectrum of the exact CNOT. This phenomenon is likely attributable to homogeneous broadening, augmented noise, and extended pulsing durations necessitated by the longer sequence.

4.2. Truth Table

Before applying the CNOT gate to obtain the truth table, state preparation is performed as discussed in our theoretical framework. The pulse se-

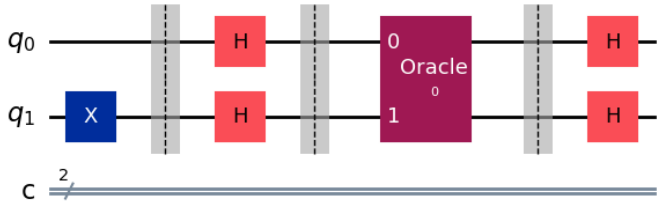

Fig. 1: Deutsch-Jozsa circuit on two-qubit quantum circuits. The oracle is responsible for implementing the classical function.

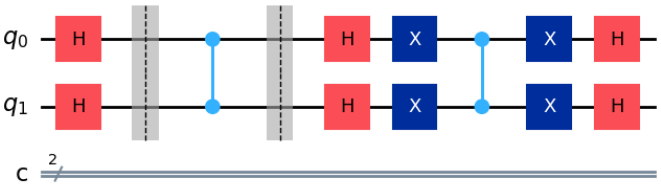

Fig. 2: Quantum circuit for Grover's algorithm, designed to identify the solution for $f(11) = 1$ and $f(x) = 0$ for all other inputs.

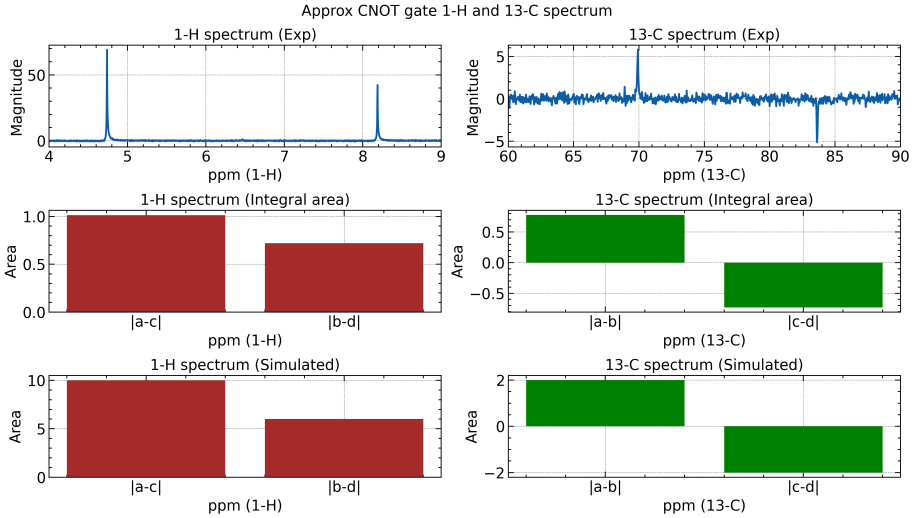

Fig. 3: Result of applying the approximate CNOT gate on the thermal state. The top plots present the frequency domain data from the experiment. The middle plots illustrate the integral of the two peaks. The bottom plots display the simulated frequency domain spectra.

quence for averaging is provided in the GitHub repository. Following state preparation, the output is recorded and presented in Figures 5. As observed from the plot, the experimentally prepared $|00\rangle$ state closely resembles the expected spectrum of the $|00\rangle$ state. Furthermore, the states $|01\rangle$, $|10\rangle$, and $|11\rangle$ are generated by applying the X gate to the respective channels [1].

Upon applying the CNOT gate to each basis state, we measure the hydrogen frequency data. To mitigate the effects of spectrum line-width, the integrals of the peaks are calculated and plotted in Python,

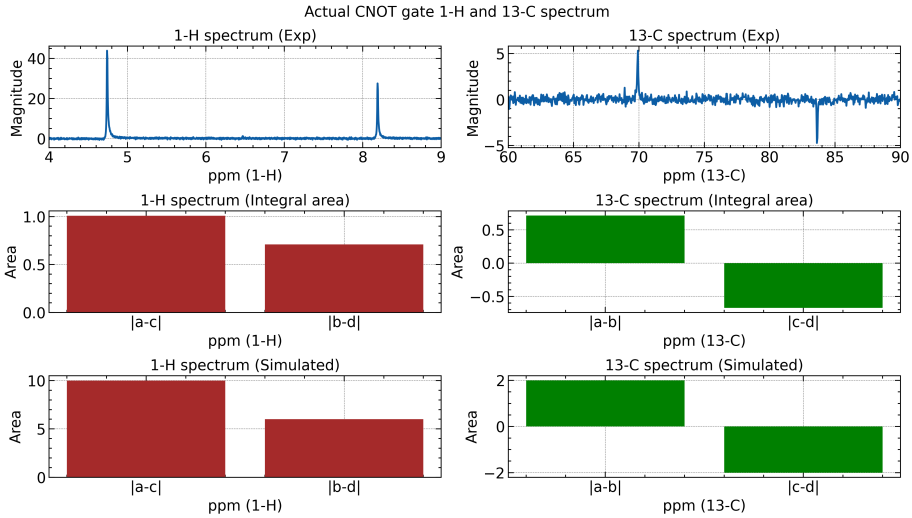

Fig. 4: Result of applying the exact CNOT gate on the thermal state. Analogous to the approximate CNOT, the top plots depict the experimental frequency domain data. The middle plots delineate the integral of the two peaks. The bottom plots convey the simulated frequency domain spectra.

as shown in Figures 6. The theoretical spectra are plotted to the left for comparison. The truth table generated from our experiment aligns with the expected behavior, although the match is not as precise as in the pseudo-pure state preparation cases. To quantify the deviation of each data point from the expected output, we calculate the ratio of the integrals of peaks between the experimental and ideal cases. The deviation ratios, using the peaks from our pseudo-pure state preparation as a benchmark, are $0.91, 0.73, 0.79, 0.65$ for $|00\rangle$, $|01\rangle$, $|10\rangle$, and $|11\rangle$, respectively.

4.3. Deutsch-jozsa experiment

We proceeded with the execution of the Deutsch-Jozsa algorithm on our Nuclear Magnetic Resonance (NMR) apparatus, adhering to the theoretical framework outlined previously. As explicated in the theory section, the Deutsch-Jozsa algorithm incorporates four distinct oracles, detailed in Table 1. The generalized circuit for executing the Deutsch-Jozsa algorithm is illustrated in Figure 1, and the implementation of each oracle is comprehensively described in the theory section. By employing the gates and pulse sequences derived, we successfully implemented all four oracle cases on our NMR machine, with the results depicted in Figure 7.

The experimental outcomes exhibit a close alignment with the patterns predicted by simulation, confirming the NMR spectrum's capability to accurately address the Deutsch-Jozsa problems for each case. However, the plots also reveal the presence of noise. To quantify the deviation of each data point from the expected outcomes, we calculated the ratio of the integrals of peaks between the experimental and ideal cases. Using the peaks from our pseudo-pure state preparation as a benchmark, the deviation ratios for the functions f_0, f_1, f_2, and f_3 were determined to be 0.86, 0.70, 0.31, and 0.55, respectively. Notably, the balanced functions exhibited more noise compared to the constant functions, a phenomenon anticipated due to the increased circuit complexity associated with balanced functions. The necessity for additional pulse sequences to implement the extra quantum gates inherently accumulates errors, leading to outputs that diverge from the ideal.

4.4. Grover Algorithm experiment

We proceeded with the implementation of Grover's algorithm on our Nuclear Magnetic Resonance (NMR) apparatus, closely adhering to the theoretical framework established beforehand. As elaborated in the theory section, Grover's algorithm is designed to identify the state x for which $f(x) = 1$. In our case, we configured the oracle to satisfy $f(11) = 1$. The circuit, customized for our specific application of Grover's algorithm, is illustrated in Figure 2. By applying the gates and pulse sequences deduced from the theoretical analysis, we successfully executed Grover's algorithm on our NMR machine, with the outcomes displayed in Figure 8.

The experimental results closely mirrored the anticipated patterns from simulations, thus confirming the capability of the NMR spectrum to facilitate quantum computing operations, including Grover's algorithm. However, we noted a significant presence of noise in the experimental data. To quantify the deviation from expected results, we assessed the ratio of the integrals of peaks between the experimental outcomes and the theoretical predictions. Using

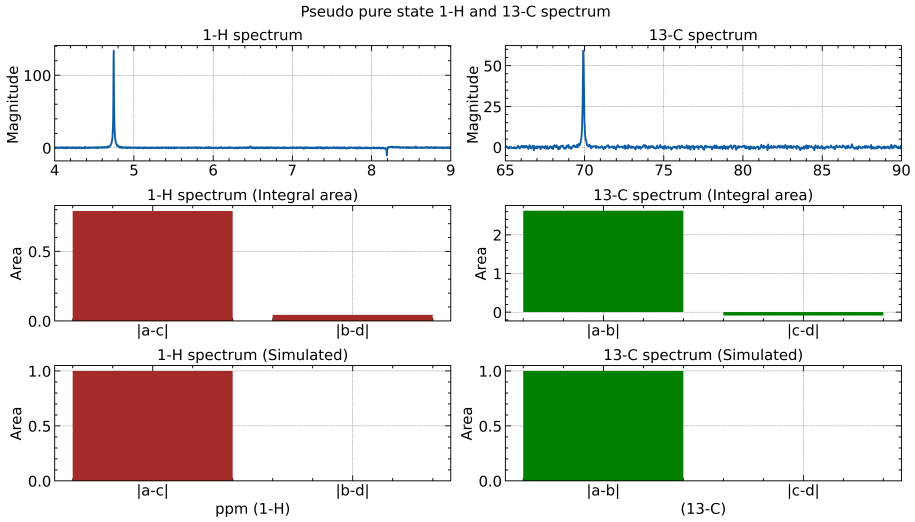

Fig. 5: This contains data about our puesdo pure state $|00\rangle$ after temporal averaging. The top plot contains the frequency domain data. The middle plots are the integral of the peaks from experiment. The bottom plots contain the theoretical plots from simulation.

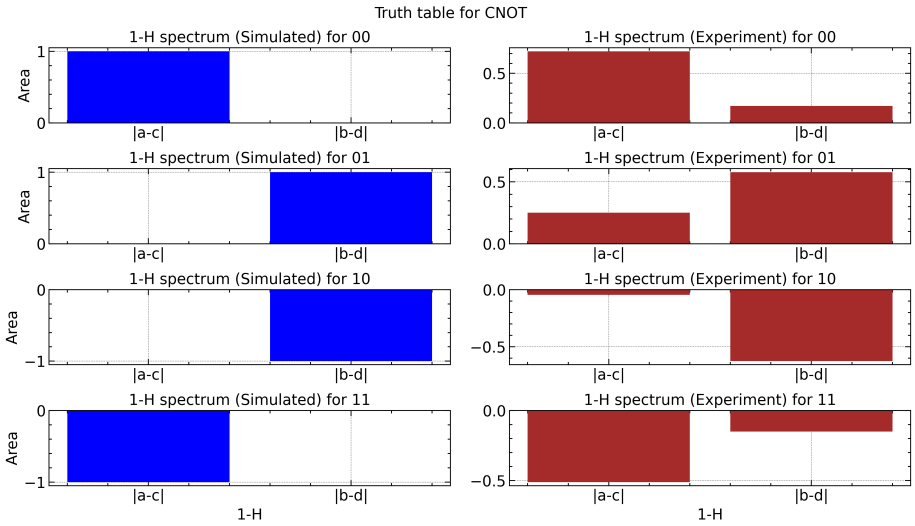

Fig. 6: The truth table containing the results of applying exact CNOT to our four basis states. The left plots show the expected result, whereas the right plots show our experiment result. Those results are the integral of our spectra data

the peaks from our pseudo-pure state preparation as a benchmark, we observed a deviation ratio of 0.45, higher than typically seen in Deutsch-Jozsa algorithm implementations, reflecting the increased complexity of Grover's circuit and the error accumulation due to additional pulse sequences.

Furthermore, to examine Grover's algorithm's periodic behavior as discussed in the theoretical section, we conducted experiments at iterations $k = 1, 2, 4, 5, 7, 8, 10$. The integral of the $b-d$ peak, corresponding to $|11\rangle$ in 1-H, is represented on the y-axis in Figure 9, showcasing the expected periodicity with maximal signal strength at iterations $k = 1, 4, 7, 10$. However, we also observe an overall decay pattern beside the periodic pattern. There might be two main reasons for the behaviour. First, the inherent inaccuracy in pulse sequences accumulates with repeated iterations. As pulses are applied in succession for multiple iterations, their inaccuracies aggregate, leading to a gradual drift from the desired quantum state. Second, the physical constraints of the NMR system, specifically T_1 relaxation and T_2^* decoherence, worsen this attenuation. As the pulsing time increases, the effect of the relaxation and decoherence on our NMR system also becomes larger.

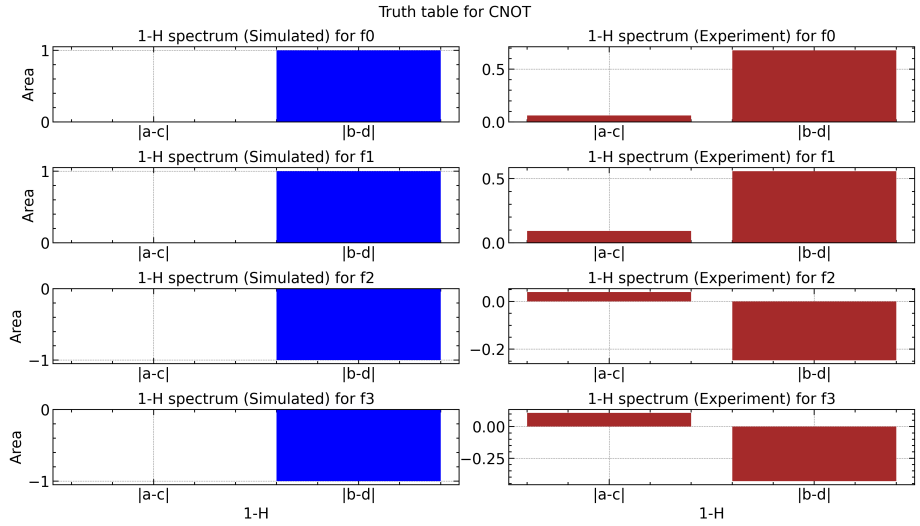

Fig. 7: The truth table containing the results of applying Deutsch-Jozsa circuit to our $|00\rangle$ state with four different oracle cases detailed in theory section. The left plots show the expected result, whereas the right plots show our experiment result. Those results are the integral of our spectra data

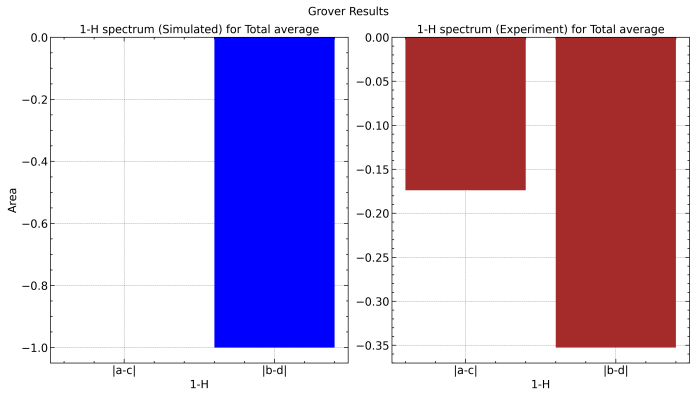

Fig. 8: Experimental and expected outcomes of applying Grover's algorithm on our $|00\rangle$ state, as depicted in Figure 2.

5. Conclusion

In this report, we have successfully demonstrated the implementation of quantum computing algorithms on a nuclear magnetic resonance (NMR) system using chloroform molecules as qubits. Through theoretical analysis and experimental validation, we have showcased the capability of NMR quantum computers to execute fundamental quantum operations and seminal quantum algorithms.

The realization of the CNOT gate, a critical building block for quantum circuits, was achieved by carefully designing and applying pulse sequences that effectively manipulate the spin states of the hydrogen and carbon nuclei in chloroform. Furthermore, we implemented the Deutsch-Jozsa algorithm, which efficiently distinguishes between constant and balanced binary functions, and Grover's search algorithm, which provides a quadratic speedup over classical approaches for searching an unsorted database. In addition, Grover's periodic behaviour is also observed by applying the algorithm for different iteration numbers.

By comparing the experimental results with theoretical simulations, we demonstrated the accuracy of our implementations, while also acknowledging the presence of noise from $T1$ and $T2^*$ and inaccuracy coming from pulse calibration. We analyze the source of these errors in a case-by-case analysis.

Despite the challenges, the successful execution of these quantum algorithms on our NMR quantum computer underscores the potential of this technology and its contribution to the broader field of quantum computing. NMR systems have played a pivotal role in the early development and experimental demonstration of quantum algorithms, paving the way for

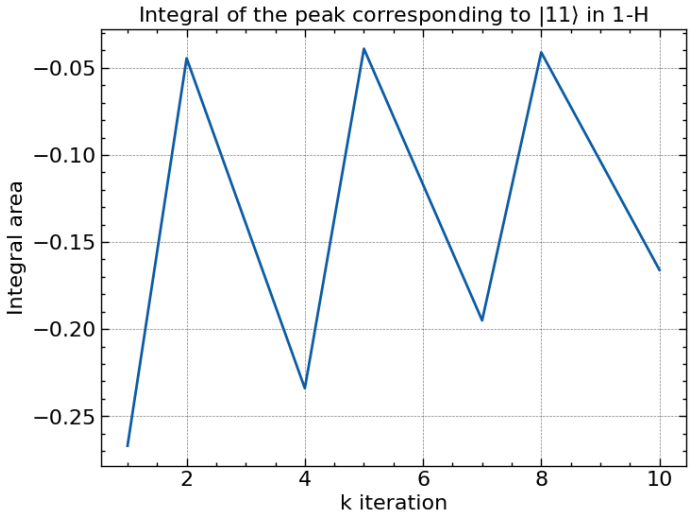

Fig. 9: Periodic behavior of Grover's algorithm demonstrated through the integral of the $b - d$ peak corresponding to $|11\rangle$ in 1-H, across different iterations.

further advancements in quantum information processing.

As we look towards the future, the insights gained from this work will inform the ongoing efforts to develop scalable and fault-tolerant quantum computers. The principles and techniques explored in this report will serve as a foundation for more advanced implementations, enabling the exploration of quantum algorithms with increasing complexity and potential applications across various scientific and computational domains.

While NMR quantum computing systems may have inherent limitations in terms of scalability, their significance lies in their ability to serve as testbeds for quantum algorithms and to facilitate a deeper understanding of the underlying principles of quantum computation. As the field of quantum computing continues to evolve, the knowledge and experience acquired through NMR implementations will pave the way for the realization of larger-scale, more powerful quantum computing technologies, ultimately unlocking the full potential of this revolutionary paradigm.

REFERENCES

[1] David Cory, Amr Fahmy, and Timothy Havel. Ensemble quantum computing by nmr spectroscopy. *Proceedings of the National Academy of Sciences of the United States of America*, 94:1634–9, 04 1997.

[2] Jonathan A. Jones. Quantum computing with nmr. *Progress in Nuclear Magnetic Resonance Spectroscopy*, 59(2):91–120, August 2011.

[3] James Keeler. *Understanding NMR Spectroscopy*. John Wiley and Sons, 2 edition, 2010. Accessed 20 Mar. 2024.

[4] E. Knill, I. Chuang, and R. Laflamme. Effective pure states for bulk quantum computation. *Physical Review A*, 57(5):3348–3363, May 1998.